Singular time-dependent photoconductivity response of $MAPbI_3$ samples deposited by vacuum processing on different substrates

*Anderzon F. Palechor-Ocampo, Jorge Caram, Pedro Hierrezuelo-Cardet, Federico Ventosinos, Daniel Pérez-del-Rey, Henk J. Bolink, Javier A. Schmidt**

Anderzon F. Palechor-Ocampo, Pedro Hierrezuelo-Cardet
Instituto de Física del Litoral (IFIS-Litoral), CONICET-UNL, Güemes 3450, S3000GLN Santa Fe, Argentina

Dr. Jorge Caram, Dr. Federico Ventosinos, Dr. Javier A. Schmidt
Instituto de Física del Litoral (IFIS-Litoral), CONICET-UNL, Güemes 3450, S3000GLN Santa Fe, Argentina and Facultad de Ingeniería Química, Universidad Nacional del Litoral, Santiago del Estero 2829, S3000AOM Santa Fe, Argentina
E-mail: javier.schmidt@santafe-conicet.gov.ar

Dr. Daniel Pérez-del-Rey, Dr. Henk J. Bolink
Instituto de Ciencia Molecular, Universidad de Valencia, C/Catedrático J. Beltrán 2, 46980 Paterna, Spain

Keywords: hybrid perovskite, photoconductivity, charge carrier dynamics, thermal evaporation

Organo-inorganic halide perovskites continue to generate enormous interest for their potential use in various optoelectronic devices. Among the different fabrication methods, vacuum thermal deposition allows uniform films over large areas, providing good material quality without using organic solvents. However, the influence of the substrate on the properties of the material deposited by vacuum processing is a point that deserves further investigation. In this work, we use time-dependent photoconductivity measurements to investigate the dynamics of charge carriers under illumination in planar films of $CH_3NH_3PbI_3$. The samples are deposited by thermal sublimation on different substrates: PbI_2, TaTm, C_{60} and glass. Experimentally, we show that the substrate has a profound effect on perovskite behavior, and that photoconductivity is sensitive enough to probe these behaviors. Furthermore, we propose a model based on Shockley-Read-Hall statistics that can explain the different photoconductivity responses by changing only the relative values of the different capture coefficients and the position of the Fermi level. We argue that the substrate changes the stoichiometry of the evaporated material, affecting the transient photoconductivity response.

1. Introduction

In the 1990s, organo-inorganic perovskites (OIP) were extensively studied both in their synthesis and their optoelectronic properties.[1–4] Almost twenty years later, the Miyasaka group proposed their incorporation as visible-light sensitizers in photoelectrochemical cells, obtaining a 3.8 % power conversion efficiency.[5] That work marked the beginning of a new phase of photovoltaic research. The use of perovskites as the active layer in photovoltaic cells turned out in a spectacular year-on-year increase in power conversion efficiency, now reaching 25.7 %.[6] This gave a very strong impetus to the development of a material that showed to be quite variable and unstable in its properties, being the instability issue probably the major drawback for the insertion of perovskite solar cells (PSC) as a new low-cost and high-performance photovoltaic technology.[7–9] Additionally, the presence of traps, recombination centers derived from chemical impurities and/or structural defects, and the singular perovskite ionic conduction, have negative implications on the device performance.

Among the several existing OIP, the most extensively studied member of this family and most commonly used as an absorber layer in PSCs is methylammonium lead tri-iodide ($CH_3NH_3PbI_3$ or $MAPbI_3$). $MAPbI_3$ has a direct bandgap of ~1.6 eV, high optical absorption coefficient, sharp absorption edge, long carrier lifetime and large diffusion lengths.[10–14] Additionally, PSCs also have significant advantages for PV technology, such as being processed from different scalable processes such as spray-deposition,[15,16] spin coating,[17,18] and vacuum deposition,[19,20] among others. The many variables involved in the preparation of OIP by spin-coating, the most popular synthesis method up to date, leads to a large variability in the properties of materials prepared by different laboratories. On the other hand, vacuum deposition provides more control over the operational variables, with samples exhibiting high crystallinity and smooth interfaces.[21] However, it is known that the substrate over which the perovskite film grows has an influence on the final properties of the material.[22,23] In PSC, the

absorber layer is grown over different transport or passivation layers, depending on the p-i-n or n-i-p architecture of the device. For the p-i-n solar cells deposited by evaporation, the combination glass/ITO/MoO_3/TaTm/$MAPbI_3$ is usually employed, where ITO is indium tin oxide, molybdenum oxide is used as a hole extraction layer, and N4,N4,N4',N4'-tetra([1,1'-biphenyl]-4-yl)-[1,1':4',1'-terphenyl]-4,4'-diamine (TaTm) is used as a hole transport layer.[19,24] TaTm is usually chosen due to its very stable sublimation conditions and tendency to form completely amorphous films.[25] For the n-i-p configuration, in most cases an inorganic oxide such as TiO_2 or SnO_2 is used. However, when such inorganic layers are employed often significant hysteresis is observed in the J-V characteristics of perovskite solar cells. To mitigate this to a large extend, very often fullerenes are employed in between the inorganic oxide and the perovskite layer. Hence, effectively the perovskite is deposited on top of a thin layer of fullerene.[26–28] On the other hand, there are many reports identifying that an excess of PbI_2 formed at the interface between the charge extracting layer and the evaporated perovskite film has effects on the eventual solar cell performance.[29,30] The influence of the substrates, especially TaTm, C_{60} and PbI_2, on the OIP properties is a subject that deserves further investigation.

Regarding characterization techniques, optical methods have been extensively used,[12,23,31,32] while conductivity measurements, although very important for PCS performance, have been less employed. Among conductivity-based techniques, impedance spectroscopy is one of the most frequently used, with very sophisticated models needed to interpret the results, but even with opposite conclusions occasionally.[33–35] On the other hand, photoconductivity measurements can provide information about the processes of charge generation, transport and recombination under illumination. Recently, Basumatary and Agarwal[36] studied these processes in $MAPbI_3$ thin films obtained by thermal evaporation and dip coating. Their study focused on the influence of temperature, illumination duration and illumination intensity on the photocurrent. The transient behavior was studied by fitting with exponential functions the

current decay curves obtained experimentally. Similarly, Gordillo *et al*.[37] reported information on carrier mechanisms that affect the trapping and recombination processes, from a fit of transient photocurrent measurements in thin films of $MAPbI_3$, $MAPbI_2Br$, and $MAPbI_2Cl$ prepared by spin coating. In both works, the rise and decay curves of the photocurrent were fitted using the method proposed by Serfaty and Joshi,[38] which assumes that the shape of the relaxation curves can be described by multiexponential terms.

In this work we propose a different methodology, which consists in solving the rate equations for free holes and electrons with a given model that takes into account the processes of trapping and recombination. Solving these differential equations for different sets of parameters allows us to qualitatively reproduce the measured behaviors. This kind of approach for studying transient photoconductivity phenomena has been used to study epitaxially grown GaN,[39,40] 4H-SiC,[41] and a-Si:H,[42] but to our knowledge it has rarely been used to study the photoconductivity of perovskite materials. Proceeding in this manner, compared to fitting with exponential functions, is preferable, since it gives more insight into the physics of recombination processes, understanding the role of different types of defects, and could allow for the interpretation of more complicated behavior (like the overshooting that will be seen in the experimental results) that may not be explained by exponential functions.

This work is organized as follows. In section 2 we will present the experimental results. Section 3 describes the model proposed and the assumptions made. In section 4 we will present the results of the theoretical model and give a proper discussion about its potential to reproduce the experimental data. In section 5 we will give the final conclusions of the manuscript. Finally, in section 6 we will give the experimental details.

2. Results

Conductivity responses of $MAPbI_3$ thin films grown over different substrates were measured. As explained in the Introduction, investigating the influence of the substrate on the

properties of the perovskite film is quite interesting because the absorber material will grow over different layers depending on the device configuration. The behavior of the four stacks studied after the switch-on or switch-off of the light, are shown in **Figure 1**. We will first concentrate on the behavior after switching on the illumination. The PbI_2/$MAPbI_3$ structure (see Figure 1a) has the most commonly observed photoconductivity response in perovskite and other semiconductor materials,[38,43] consisting of a rapid increase in the first seconds of illumination, followed by a smoother increase that tends to a stable value. The drastic increase of conductivity observed in the PbI_2/$MAPbI_3$ film as soon as the light is switched on, can easily be attributed to the quick generation of electron-hole pairs due to the absorption of photons having energies comparable to or larger than the bandgap energy. The stabilization that follows is due to a balance between generation and recombination, leading to a steady-state situation. It is interesting to note the time scale of the stabilization process, since it takes around 2200 s for the conductivity to reach a constant value of $\sim 1.1 \times 10^{-5}$ $\Omega^{-1}cm^{-1}$. The dark conductivity, which corresponds to the first point in Figure 1 a), is 2×10^{-8} $\Omega^{-1}cm^{-1}$, corresponding to a huge photoconductivity gain of ~ 550.

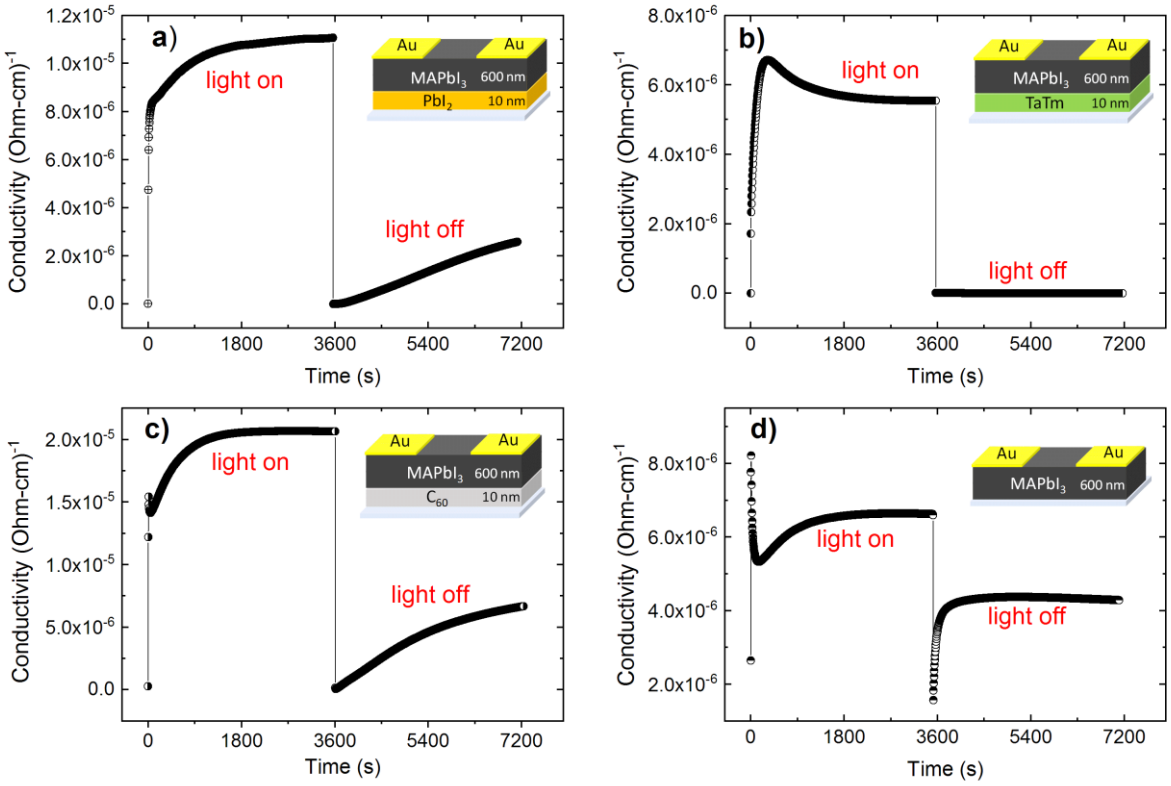

Figure 1. Conductivity responses of thin films of PbI_2/$MAPbI_3$, TaTm/$MAPbI_3$, C_{60}/$MAPbI_3$ and glass/$MAPbI_3$.

On the other hand, TaTm / MAPBi3 films (see Figure 1b) exhibit a slower increase in photoconductivity in the first instances of illumination, which continues to increase continuously until it reaches a maximum value around t = 300 s. After achieving this maximum value, the response decays, first rapidly and then more slowly, until reaching a stationary value. This characteristic behavior is known as overshooting, and it was previously observed in $MAPbI_3$ perovskite films[36,37] and in MAPbX3 (X = I, Br, Cl) single crystals.[44,45] Clearly, an interplay between different capture and recombination processes is taking place in these samples, to produce such a particular behavior.

Finally, the last two samples, with C_{60} (see Figure 1c) or glass (see Figure 1d) as substrates, show an almost instantaneous increase (for the time scales of our measurements) in the photoconductivity at the first seconds of illumination. After this sharp rise, both samples show a peculiar behavior that, to the best of our knowledge, has not been reported so far. The conductivity decreases during illumination, reaches a minimum value, and then gradually

increases until reaching a stable value. The difference between both samples is the magnitude of the initial rise, which in the C_{60}/$MAPbI_3$ sample is lower and in the glass/$MAPbI_3$ sample is higher than the final steady-state value; but this difference may be due to the time resolution of our measurements. In any case, this complex behavior is related to different competing trapping and recombination channels.

The creation of new recombination centers caused by injected carriers is a possibility that has been pointed out by some authors.[46] This process could have an influence on the time dependence of the photoconductivity curves; however, the creation of recombination centers would cause a slow decrease of the photoconductivity due to the increased recombination rate, something that is only observed in Figure 1 b) but not for the other structures. To gain more insight into the observed phenomena, we propose a model based on Shockley-Read-Hall theory,[47,48] which will be discussed in the next section.

After turning off the light, conductivity responses show three different behaviors (see Figure 1). In the first one (PbI_2/$MAPbI_3$ and C_{60}/$MAPbI_3$ films), the conductivity initially decays rapidly to the original dark value, followed by a constant increase that is not observed to saturate after an hour under dark conditions. In the second behavior (TaTm/$MAPbI_3$ film), the conductivity returns to the original dark value and remains unchanged. Finally, the conductivity of the glass/$MAPbI_3$ film shows an initially drastic drop to a value even lower than the original dark value, followed by a quick increase and reaching a stable value different from the initial one. A discussion will be given in Section 5 about the possibility of the proposed model to reproduce also the dark conductivity trends.

3. Theoretical Model

A model based on Shockley-Read-Hall theory is proposed to describe the photoconductivity measurements over symmetrically contacted $MAPbI_3$ films. We propose a trap-mediated recombination model, with a single recombination center for electrons and holes located around

the middle of the gap **(Figure 2)**. The time-dependent variables are the concentration of electrons in the conduction band (CB), $n(t)$, the concentration of holes in the valence band (VB), $p(t)$, and the concentration of electrons in the recombination center (RC), $n_r(t)$.

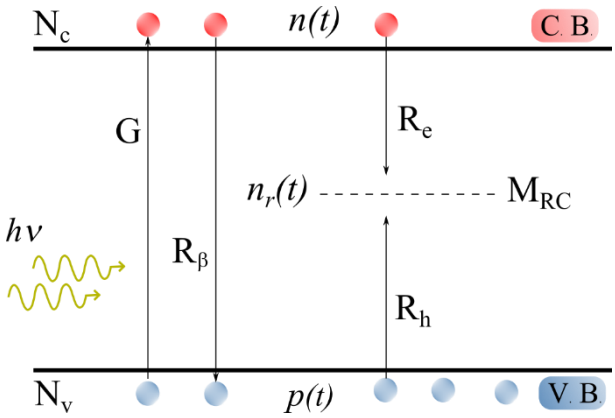

Figure 2. Sketch of the proposed kinetic model to describe the photoconductivity experimental behaviors. The model considers a white light excitation with a generation rate *G*, a band-to-band recombination rate R_β, and capture rates for electrons and holes R_e and R_h, respectively. The total trap density of states is M_{RC} (acceptor states), and the three variables considered in the model are *n(t)*, $n_r(t)$ and *p(t)*, namely electrons in the CB, electrons in trap states and holes in the VB, respectively.

The component of the white light excitation with $h\nu > 1.6$ eV produces a generation rate of electrons and holes $G = \psi(N_V - p)(N_C - n)$, where the coefficient ψ is associated with the convolution matrix of the optical transitions between the occupied initial states $(N_V - p)$ and the unoccupied final states $(N_C - n)$. N_V and N_C are the effective densities of states for the VB and the CB, respectively, which were extracted from the literature.[49] The model assumes two recombination channels. One is the band-to-band recombination, giving a recombination rate $R_\beta = \beta\, n(t)\, p(t)$, where β is the bimolecular recombination coefficient. The other recombination channel is through RCs, which are assumed to have an energetic position $E_{RC} =$ 0.6 eV above the valence band edge and a total density M_{RC}. The energetic position E_{RC} is chosen according to the results of Eames *et al.*[50], who used first principles calculations to estimate this energy, and Levine *et al.*[42], who found this position based on experimental considerations. We assume the trap level to be of acceptor type: neutral when empty and

negative when occupied. Recombination centers capture electrons at a rate $R_e = c_n\, n(t)\, [M_{RC} - n_r(t)]$, where c_n is the capture coefficient for electrons, and the rate is proportional to the concentration of electrons in the conduction band, $n(t)$, and the concentration of holes in the recombination center, $[M_{RC} - n_r(t)]$. In a similar fashion, RCs also capture holes at a rate $R_h = c_p\, p(t)\, n_r(t)$, where c_p is the capture coefficient for holes, and the rate is proportional to the concentration of holes in the valence band, $p(t)$, and the concentration of electrons in the recombination center, $n_r(t)$. Therefore, the balance equations that rule the evolution of $n(t)$, $p(t)$, and $n_r(t)$ are

$$\frac{dn}{dt} = \psi(N_v - p)(N_c - n) - \beta\, n\, p - c_n\, n\, (M_{RC} - n_r)\,, \tag{1}$$

$$\frac{dn_r}{dt} = c_n\, n\, (M_{RC} - n_r) - c_p\, p\, n_r\,, \tag{2}$$

$$\frac{dp}{dt} = \psi(N_v - p)(N_c - n) - \beta\, n\, p - c_p\, p\, n_r\,. \tag{3}$$

The model has the following implicit assumptions: i) the space charge is negligible, considering ideal ohmic contacts (experimentally checked, see Figure S1); ii) there is no carrier concentration gradient (no diffusion), i.e., excitation produces a homogeneous excess of carrier in the bands; and iii) thermal reemission from traps to the bands is assumed to be negligible due to the energetic position of the RC close to the middle of the gap (deep trap).

A similar model to describe trapping and recombination in perovskite materials has already been proposed in the literature.[49,51,52] In addition, we have verified that the addition of more recombination channels does not provide a better description of the experimental curves, leading us to conclude that this is the simplest model that can reproduce the illumination curves, as will be seen in the next section.

Simulations were developed in three parts. First, we calculate the dark equilibrium concentrations n_0, p_0 and n_{r0} from the Fermi level position E_F, which is considered one of the free parameters of the model, from the equations

$$n_0 = N_C\, e^{-\frac{(E_C - E_F)}{kT}}, \quad (4)$$

$$p_0 = N_V\, e^{-\frac{(E_F - E_V)}{kT}}, \quad (5)$$

$$n_{r0} = \frac{M_{RC}}{1 + e^{\frac{E_{RC} - E_F}{kT}}}\ . \quad (6)$$

Second, under illumination conditions (G>0), we use the concentrations found under dark equilibrium (n_0, p_0 and n_{r0}) as the initial values to be used in the coupled system of nonlinear differential equations, **Equation 1-3**, which is solved numerically. Finally, we use the last value of the concentrations under illumination as an initial condition for the evolution of the system without illumination (G=0). The main goal of the model is to reproduce qualitatively the experimental behaviors observed, in order to infer the temporal evolution of the carriers on the real physical system. The free parameters that are adjusted are the Fermi level position E_F and the coefficients β, c_n and c_p. Equation 1-3 are normalized to the value of M_{RC}, which is unknown. Furthermore, the value of the transition matrix element ψ is unknown. Therefore, the conductivity that we obtain is arbitrary in our model and is normalized to one.

4. Discussion

Figure 3 shows the experimental photoconductivity responses and the simulation using the model described in Section 4, both normalized to one at the steady-state value. We have obtained the four different photoconductivity responses by adjusting the parameters E_F, β, c_n and c_p (see **Table 1**). As mentioned above, the simulation is qualitative and uses its own photoconductivity scale; despite this, the model reproduces all the features of the four photoconductivity responses. Starting with the PbI_2/$MAPbI_3$ film (see Figure 3a), to achieve the quick increase of conductivity in the first stages of illumination followed by a progressive stabilization, β is the dominating recombination coefficient (almost two orders of magnitude larger than the holes capture coefficient c_p). The energetic position of the recombination center and the concentration of external dopants lead to a Fermi level located at $E_F = 0.86$ eV above

E_V. The slight n-type character of this sample deposited on PbI_2 is consistent with experimental findings that observe n-type doping for PbI_2-rich materials.[53] The dominance of band-to-band recombination is the simplest explanation for the monotonic increase in conductivity after switching on illumination, with a recombination rate $R_\beta = \beta\, n(t)\, p(t)$ gradually increasing as the carrier concentrations increase, until balancing the generation rate.

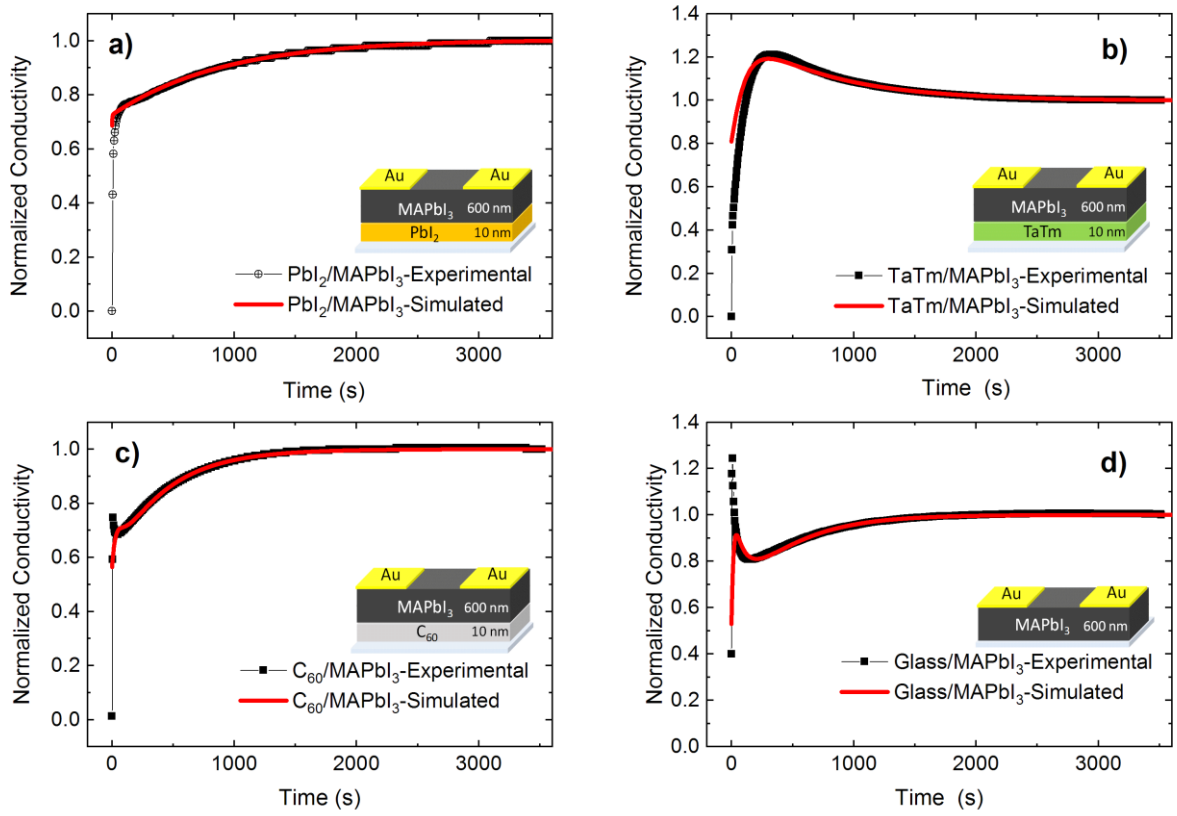

Figure 3. Comparison between experimental and simulated photocurrent curves for thin films of a) PbI_2/$MAPbI_3$, b) TaTm/$MAPbI_3$, c) C_{60}/$MAPbI_3$ and d) Glass/$MAPbI_3$.

	E_F [eV]	β [cm^3s^{-1}]	c_n [cm^3s^{-1}]	c_p [cm^3s^{-1}]
PbI_2/$MAPbI_3$	0.86	1.34×10^{-5}	1.47×10^{-8}	4.04×10^{-7}
Glass/$MAPbI_3$	0.77	4.57×10^{-6}	3.32×10^{-8}	8.39×10^{-8}
C_{60}/$MAPbI_3$	0.75	9.62×10^{-7}	8.13×10^{-9}	2.24×10^{-7}
TaTm/$MAPbI_3$	0.71	6.89×10^{-8}	8.62×10^{-9}	5.15×10^{-9}

Table 1. Values of the Fermi level E_F (referred to the valence band edge), the bimolecular recombination coefficient β, the electron capture coefficient c_n, and the hole capture coefficient c_p, that reproduce the experimental photocurrent responses.

For the TaTm/$MAPBI_3$ sample (Figure 3b), the external dopant concentration leads to a Fermi level located at $E_F = 0.71$ eV above E_V. To reproduce the overshooting seen experimentally, the capture coefficients for electrons and holes become comparable to β, with $c_n > c_p$. For the C_{60}/$MAPbI_3$ sample (Figure 3c), the Fermi level position is $E_F = 0.75$ eV above E_V, and $\beta \sim 4\, c_p > c_n$. Finally, for the Glass/$MAPbI_3$ sample (Figure 3d) the Fermi level position is $E_F = 0.77$ eV above E_V, and β is again much larger than c_n or c_p.

For the samples studied, the position of the Fermi level varies with the substrate used in the following way: $E_F = 0.71$ eV for TaTm, 0.75 eV for C_{60}, 0.77 eV for Glass, and 0.86 eV for PbI_2. Since the samples are deposited by vacuum sublimation from two sources, CH_3NH_3I and PbI_2, the growth of the perovskite depends on the relative sticking coefficient of the species on the substrate. Comparing TaTm with C_{60} substrates, we have observed from X-rays diffraction (XRD) that the perovskite deposited over C_{60} is less crystalline and exhibits a significant amount of crystalline PbI_2 (see Figure S2). For the sample deposited over glass, we also expect an excess of PbI_2 in the composition, since we have observed a lower sticking coefficient for CH_3NH_3I than for PbI_2 over bare glass.[22,30] Finally, for the sample deposited over PbI_2, this compound from the substrate is probably incorporated into the bulk of the perovskite during the growing process. Therefore, the position of the Fermi energy is correlated with the excess of PbI_2 in the perovskite, with the Fermi level moving toward the conduction band as the sample is enriched in PbI_2. These results agree with those of Wang *et al.*, who showed that PbI_2-rich films are n-doped and PbI_2-deficient films are p-doped.[53] We conclude that the substrate has an influence on the stoichiometry of the $MAPbI_3$ samples deposited by vacuum evaporation, changing therefore the electrical properties. The position of the Fermi level is also correlated with the band-to-band recombination coefficient, since we observe the sequence $\beta_{PbI2} > \beta_{Glass} > \beta_{C60} > \beta_{TaTm}$, meaning that β increases as the concentration of

PbI_2 in the perovskite increases and the Fermi level moves towards the conduction band (see **Table 1**). We attribute the increase of β to a decrease in the concentration of recombination centers within the gap of the material. Since it is believed that the main defect of the perovskite is the iodine vacancy, V_I, the excess of PbI_2 will tend to fill these vacancies, thus reducing the number of recombination centers. Therefore, the shift of the Fermi level is correlated to the increase of the band-to-band recombination rate. The increase of β means a larger probability of radiative recombination, and is also consistent with the measured dependence of the photoluminescence quantum yield (PLQY). Indeed, we have observed that a TaTm substrate quenches the luminescence, while the PLQY increases for substrates of C_{60} or glass (see Figure S3).

In order to get more insight into the carrier's dynamics, we have used the numerical simulations to track the populations of electrons, holes, and trapped charge as a function of time, studying the influence of the parameters on the different recombination channels. As an example, we will analyze the behavior of the TaTm/$MAPbI_3$ sample. The analysis of the other samples can be found in the supporting information.

As stated in section 3, the simulations begin by solving the charge neutrality equation for dark equilibrium conditions, finding the position of the Fermi level that gives equal concentrations of positive and negative charges. For the simulation of the sample deposited over TaTm, the Fermi level lies at 0.71 eV above the valence band edge, consistent with the slightly p-type character of the sample. **Figure 4a** shows the evolution of the concentrations of free holes (p, blue curve), free electrons (n, red curve) and trapped electrons (n_r, green curve) as a function of time, after switching on the illumination at t = 0 s and switching off the illumination at t = 3600 s. The concentrations have been normalized to the maximum value. At $t \leq 0$ s, p is much larger than n (due to the p-type character of the sample), and n_r is even greater as the position of the recombination centers (E_{RC} = 0.60 eV) lies below the dark Fermi level, so

these states are mainly occupied by electrons. The extra positive charge to maintain charge neutrality is provided by ionized donors.

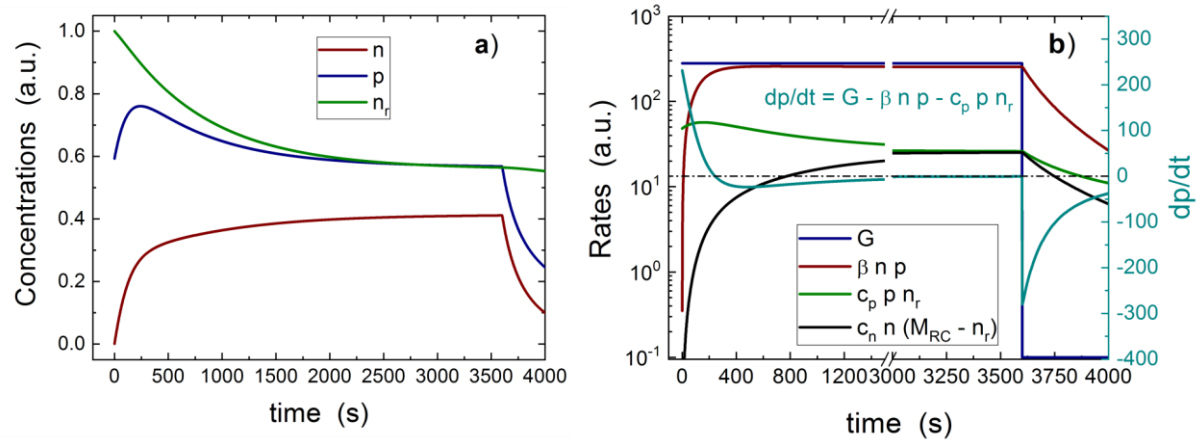

Figure 4: a) Evolution of the concentrations of free holes (p), free electrons (n) and trapped electrons (n_r) as a function of time. b) Evolution with time of the generation rate (G), the band-to-band recombination rate ($\beta\ n\ p$), the recombination rate of holes through gap states ($c_p\ p\ n_r$), and the recombination rate of electrons through gap states ($c_n\ n\ [M_{RC} - n_r]$) (left axis), and time derivative of the free holes concentration (dp/dt, right axis).

When illumination begins at $t = 0$, n and p begin to increase due to a higher generation rate than the recombination rate. This can be observed in Figure 4b, where the different rates of the balance equations have been plotted as a function of time. The interplay between the generation rate (G, blue curve) and the different recombination channels determines the evolution of the concentrations. At $t = 0$ s, G is larger than the band-to-band recombination rate ($\beta\ n\ p$, red curve) plus the recombination rate of holes through gap states ($c_p\ p\ n_r$, green curve); therefore, p begins to increase. That can be seen in the right-hand axis of Figure 4b, where dp/dt is positive at $t = 0$ s. When illumination begins, the main recombination channel for holes is through the recombination centers ($c_p\ p\ n_r > \beta\ n\ p$), basically because $n_r >> n$. On the other hand, the recombination rate of electrons through the gap states [$c_n\ n\ (M_{RC} - n_r)$, black curve of Figure 4b] is very low at $t = 0$ s, due to the low concentrations of electrons in the conduction band and holes in the recombination centers. Therefore, $G >> \beta\ n\ p + c_n\ n\ (M_{RC} - n_r)$, and the concentration of free electrons starts to increase sharply at $t = 0$ s.

The initial increase of *n* and *p* causes that the band-to-band recombination rate increases, and the recombination channel for holes switches to band-to-band recombination (crossing between red and green curves in Figure 4b at $t \approx 37$ s). Eventually, the recombination of holes exceeds the generation rate: $G < \beta\, n\, p + c_p\, p\, n_r$. At that point (around $t = 244$ s), *dp/dt* starts to be negative and *p* starts to decrease (Figure 4a). This peak in the concentration of free holes lead to the overshooting of the photocurrent observed experimentally in Figure 3b. On the other hand, the recombination rate of electrons always remains lower than the generation rate, so the concentration of free electrons constantly increases during illumination, although always remaining lower than the concentration of holes (Figure 4a). Therefore, the behavior of the conductivity is explained by the evolution of the free-hole concentration. Finally, the concentration of trapped electrons (n_r) monotonically decreases due to the capture of holes by these recombination centers.

Around $t = 3500$ s a steady-state is reached, where the concentrations tend to a constant value (Figure 4a) and dp/dt (as well as dn/dt) tend to zero (Figure 4b). Therefore, from Equation 1 and 3 we have $G = R_\beta + R_n = R_\beta + R_p$, meaning that $R_n = R_p$ (green and black curves tend to be equal in Figure 4b). Moreover, $R_\beta \gg R_n = R_p$, so band-to-band recombination is the main recombination channel.

When the illumination is switched off at $t = 3600$ s, the recombination rates are automatically higher than the generation rate (which goes to zero), so the concentrations of both free electrons and holes tend to decrease monotonically. The dynamics for the other substrate configurations is available in the supporting information.

So far, we have been able to reproduce and explain the behavior found for the illumination stages. However, as shown in Figure 1, the evolution of dark conductivity after turning off the illumination is not trivial. After the expected decrease in conductivity just after turning off the light, three of the four sample configurations showed an increase in conductivity,

two of them (Figure 1a and Figure 1c) did not reach a steady value after an hour in dark conditions, while the remaining sample (MAPI over glass, Figure 1d) started with a sharp increase of dark conductivity that rapidly converged to a steady value. The remaining configuration (Figure 1b) is the only one that shows a monotonic decrease in conductivity. We have investigated whether the model proposed in this paper is able to reproduce these evolutions. First, we have tried to find a set of parameters (E_F, β, c_n and c_p) that could give a good overall fit. This procedure did not give the expected results; hence, we tried to only fit the dark evolutions. Despite this simplification, we have found that this model can only reproduce the decreasing dark conductivity (Figure 1b). This clearly shows a limit of what the model is able to reproduce and explain. Our hypothesis is that after turning off the light, the presence of the active electric field may have some impact on the redistribution of charges inside the perovskite material, which can lead to changes in conductivity, a phenomenon known in this material.[54] If this is the case, the model cannot simulate this type of behavior. This limitation opens up the possibility of modifying the model to include a redistribution of charges, a topic that will be studied in future works.

5. Conclusion

Conductivity responses of $MAPbI_3$ thin films evaporated over different substrate layers were studied. The experiments show that the substrate indeed has a large effect on the behavior of the perovskite film, and photoconductivity is a sensitive tool for exploring these behaviors. The PbI_2/$MAPbI_3$ sample shows a monotonous increase in conductivity after switching on the illumination, the TaTm/$MAPbI_3$ sample shows an overshooting, while the C_{60}/$MAPbI_3$ and glass/$MAPbI_3$ show an undershooting, a behavior that, to our knowledge, has not been observed before. We were able to explain the different photoconductivity responses with a very simple model based on Shockley-Read-Hall statistics, changing only the relative values of the different capture coefficients and the position of the Fermi level. Our experiments, and the interpretation

of them based on the proposed model, point to a description of the perovskite defect structure by a single trap located around midgap. Our results also show that, in the steady-state under illumination, band-to-band recombination is the main recombination channel for the samples studied. Despite the excellent qualitative agreement between the results of our model and the experimental curves, more work is needed to obtain a quantitative description of both the illumination and dark cycles.

6. Experimental Section/Methods

Sample preparation: Glass substrates were purchased from Naranjo Substrates. N4,N4,N4′,N4′-tetra([1,1′-biphenyl]-4-yl)-[1,1′:4′,1′-terphenyl]-4,4′-diamine (TaTm) was provided by Novaled GmbH, and fullerene (C_{60}) together with PbI_2 were purchased from Sigma Aldrich. CH_3NH_3I (MAI) was purchased from Lumtec. The glass substrates were cleaned with soap, deionized water, and isopropanol under an ultrasonic bath, followed by a UV-O_3 treatment. The samples were transferred to a vacuum chamber inside a N_2-filled glovebox for the deposition of the different layers. Four sets of samples were grown in the same batch, with structures i) glass/PbI_2/$MAPbI_3$, ii) glass/TaTm/$MAPbI_3$, iii) glass/C_{60}/$MAPbI_3$ and iv) glass/$MAPbI_3$. The vacuum-deposition method has been described previously.[19] Summarizing, the precursor powders were deposited separately in ceramic crucibles, that were heated up in high vacuum using Creaphys sources until the materials start subliming. Working with quartz microbalance sensors allows us to accurately control the evaporation rate of each component. For the PbI_2, TaTm and C_{60} layers the thickness was 10 nm. For the deposition of $MAPbI_3$, methylammonium iodide (CH_3NH_3I) and lead (II) iodide (PbI_2) were used in stoichiometric amounts. Controlling the perovskite thickness with a third sensor near the substrate, we prepared 600-nm-thick films. The samples were transferred to another vacuum chamber to deposit gold pads for contact. In this chamber the working principle for evaporation is similar but the heat is achieved by

applying a high current input through a tungsten boat with gold beads. Finally, the samples were encapsulated with Al_2O_3 deposited by atomic layer deposition (ALD).

Electrical measurements: Photoconductivity measurements were carried out with the samples placed inside a cryostat pumped to a pressure of 10^{-6} Torr. A constant voltage of 20 V was applied between the gold coplanar contacts, which were separated by 2 mm. The samples were subjected to one-hour symmetric light and dark cycles. In all cases, before starting each experiment the samples were kept in the dark for 30 minutes with the voltage applied, in order to stabilize the conditions before the measurements. For the illumination cycles, a 6 W LED lamp was used, without IR component to avoid heating the samples. This illumination induces an almost identical generation rate in all the samples, due to the fact that the absorption coefficients are similar in the emission region of the lamp (see Figure S5). Temperature was controlled and the samples remained at room temperature during the experiments. Dark- and photo-currents were measured with a Keithley 617 system electrometer, with data recorded every 5 s.

Supporting Information
Supporting Information is available from the Wiley Online Library or from the author.

Acknowledgements
The research leading to these results has received funding from the Argentinean National Scientific and Technical Research Council (CONICET) Project No. PUE 22920160100054CO, the Argentinian National Agency for Science and Technology Promotion (ANPCyT) (Nos. PICT-2016-1389 and PICT-2018-01614), the Litoral National University (UNL) (No. CAI + D 50420150100108L), the Spanish Ministry of Science, Innovation and Universities (Nos. MAT2017-88821-R and EQC2018-004888-P), and the Comunitat Valenciana (No. IDIFEDER/2018/061). Author 1 and Author 2 contributed equally to this work.

Received: ((will be filled in by the editorial staff))
Revised: ((will be filled in by the editorial staff))
Published online: ((will be filled in by the editorial staff))

References

[1] D. B. Mitzi, In *Progress in Inorganic Chemistry* (Ed.: Karlin, K. D.), John Wiley & Sons, Inc., Hoboken, NJ, USA, **2007**, pp. 1–121.
[2] M. Era, S. Morimoto, T. Tsutsui, S. Saito, *Appl. Phys. Lett.* **1994**, *65*, 676.
[3] N. Onoda-Yamamuro, T. Matsuo, H. Suga, *Journal of Physics and Chemistry of Solids* **1992**, *53*, 935.
[4] A. Poglitsch, D. Weber, *J. Chem. Phys.* **1987**, *87*, 6373.
[5] A. Kojima, K. Teshima, Y. Shirai, T. Miyasaka, *Journal of the American Chemical Society* **2009**, *131*, 6050.
[6] NREL, *Chart of Best Research-Cell Efficiencies:*, **2022**.
[7] P. Hierrezuelo-Cardet, A. F. Palechor-Ocampo, J. Caram, F. Ventosinos, D. Pérez-Del-Rey, H. J. Bolink, J. A. Schmidt, *J. Appl. Phys.* **2020**, *127*, 235501.
[8] P. Holzhey, P. Yadav, S.-H. Turren-Cruz, A. Ummadisingu, M. Grätzel, A. Hagfeldt, M. Saliba, *Materials Today* **2019**, *29*, 10.
[9] P. K. Nayak, S. Mahesh, H. J. Snaith, D. Cahen, *Nat Rev Mater* **2019**, *4*, 269.
[10] I. Mesquita, L. Andrade, A. Mendes, *Renewable and Sustainable Energy Reviews* **2018**, *82*, 2471.
[11] S. D. Stranks, G. E. Eperon, G. Grancini, C. Menelaou, M. J. P. Alcocer, T. Leijtens, L. M. Herz, A. Petrozza, H. J. Snaith, *Science* **2013**, *342*, 341.
[12] J. Caram, M. Senno, L. Cencha, S. Tinte, R. Urteaga, R. D. Arce, *J. Phys. D: Appl. Phys.* **2021**, *55*, 115303.
[13] S. De Wolf, J. Holovsky, S.-J. Moon, P. Löper, B. Niesen, M. Ledinsky, F.-J. Haug, J.-H. Yum, C. Ballif, *J. Phys. Chem. Lett.* **2014**, *5*, 1035.
[14] V. Gonzalez-Pedro, E. J. Juarez-Perez, W.-S. Arsyad, E. M. Barea, F. Fabregat-Santiago, I. Mora-Sero, J. Bisquert, *Nano Lett.* **2014**, *14*, 888.
[15] D. K. Mohamad, J. Griffin, C. Bracher, A. T. Barrows, D. G. Lidzey, *Adv. Energy Mater.* **2016**, *6*, 1600994.
[16] M.-Y. Cho, S. Kim, I.-S. Kim, E.-S. Kim, Z.-J. Wang, N.-Y. Kim, S.-W. Kim, J.-M. Oh, *Advanced Functional Materials* **2020**, *30*, 1907449.
[17] C. Aranda, J. Bisquert, A. Guerrero, *J. Chem. Phys.* **2019**, *151*, 124201.
[18] F. Li, J. Yuan, X. Ling, Y. Zhang, Y. Yang, S. H. Cheung, C. H. Y. Ho, X. Gao, W. Ma, *Advanced Functional Materials* **2018**, *28*, 1706377.
[19] D. Pérez-del-Rey, L. Gil-Escrig, K. P. S. Zanoni, C. Dreessen, M. Sessolo, P. P. Boix, H. J. Bolink, *Chem. Mater.* **2019**, *31*, 6945.
[20] T. Abzieher, T. Feeney, F. Schackmar, Y. J. Donie, I. M. Hossain, J. A. Schwenzer, T. Hellmann, T. Mayer, M. Powalla, U. W. Paetzold, *Advanced Functional Materials* **2021**, *31*, 2104482.
[21] D. Pérez-del-Rey, P. P. Boix, M. Sessolo, A. Hadipour, H. J. Bolink, *J. Phys. Chem. Lett.* **2018**, *9*, 1041.
[22] S. Olthof, K. Meerholz, *Sci Rep* **2017**, *7*, 40267.
[23] K. Sveinbjörnsson, K. Aitola, X. Zhang, M. Pazoki, A. Hagfeldt, G. Boschloo, E. M. J. Johansson, *J. Phys. Chem. Lett.* **2015**, *6*, 4259.
[24] A. Babaei, C. Dreessen, M. Sessolo, H. J. Bolink, *RSC Adv.* **2020**, *10*, 6640.
[25] Y. Yao, C. Cheng, C. Zhang, H. Hu, K. Wang, S. De Wolf, *Advanced Materials* **2022**, *34*, 2203794.
[26] L.-L. Deng, S.-Y. Xie, F. Gao, *Adv. Electron. Mater.* **2018**, *4*, 1700435.
[27] C. Momblona, L. Gil-Escrig, E. Bandiello, E. M. Hutter, M. Sessolo, K. Lederer, J. Blochwitz-Nimoth, H. J. Bolink, *Energy Environ. Sci.* **2016**, *9*, 3456.
[28] V. M. Le Corre, M. Stolterfoht, L. Perdigón Toro, M. Feuerstein, C. Wolff, L. Gil-Escrig, H. J. Bolink, D. Neher, L. J. A. Koster, *ACS Appl. Energy Mater.* **2019**, *2*, 6280.
[29] T. Li, M. Ren, Y. Zhang, L. Fang, J. Zhang, Y. Yuan, J. Zhang, P. Wang, *Small* **2020**, *16*, 2001866.

[30] H. Xu, Y. Wu, J. Cui, C. Ni, F. Xu, J. Cai, F. Hong, Z. Fang, W. Wang, J. Zhu, L. Wang, R. Xu, F. Xu, *Phys. Chem. Chem. Phys.* **2016**, *18*, 18607.
[31] M. E. Calvo, *J. Mater. Chem. A* **2017**, *5*, 20561.
[32] A. M. A. Leguy, P. Azarhoosh, M. I. Alonso, M. Campoy-Quiles, O. J. Weber, J. Yao, D. Bryant, M. T. Weller, J. Nelson, A. Walsh, M. van Schilfgaarde, P. R. F. Barnes, *Nanoscale* **2016**, *8*, 6317.
[33] D. A. Jacobs, H. Shen, F. Pfeffer, J. Peng, T. P. White, F. J. Beck, K. R. Catchpole, *Journal of Applied Physics* **2018**, *124*, 225702.
[34] D. Moia, I. Gelmetti, P. Calado, W. Fisher, M. Stringer, O. Game, Y. Hu, P. Docampo, D. Lidzey, E. Palomares, J. Nelson, P. R. F. Barnes, *Energy Environ. Sci.* **2019**, *12*, 1296.
[35] J. Caram, M. García-Batlle, O. Almora, R. D. Arce, A. Guerrero, G. Garcia-Belmonte, *Appl. Phys. Lett.* **2020**, *116*, 183503.
[36] P. Basumatary, P. Agarwal, *J Mater Sci: Mater Electron* **2020**, *31*, 10047.
[37] G. Gordillo, C. A. Otálora, M. A. Reinoso, *J Mater Sci: Mater Electron* **2018**, *29*, 4276.
[38] A. Serfaty, N. V. Joshi, *Phys. Rev. B* **1990**, *41*, 8545.
[39] K. Moazzami, T. E. Murphy, J. D. Phillips, M. C.-K. Cheung, A. N. Cartwright, *Semicond. Sci. Technol.* **2006**, *21*, 717.
[40] M. Salis, A. Anedda, F. Quarati, A. J. Blue, W. Cunningham, *Journal of Applied Physics* **2005**, *97*, 033709.
[41] M. Suproniuk, P. Kamiński, R. Kozłowski, M. Pawłowski, *Acta Phys. Pol. A* **2014**, *125*, 1042.
[42] J. A. Schmidt, D. M. Goldie, *Thin Solid Films* **2020**, *696*, 137793.
[43] G. Gordillo, C. A. Otálora, A. A. Ramirez, *Phys. Chem. Chem. Phys.* **2016**, *18*, 32862.
[44] P. Lin, Q. Meng, H. Chen, H. Hu, D. Fang, L. Xu, P. Wang, C. Cui, *J. Phys.: Condens. Matter* **2021**, *33*, 285703.
[45] S. Reynolds, A. R. Houghton, D. J. Keeble, *J. Phys.: Conf. Ser.* **2019**, *1186*, 012035.
[46] S. T. Birkhold, J. T. Precht, H. Liu, R. Giridharagopal, G. E. Eperon, L. Schmidt-Mende, X. Li, D. S. Ginger, *ACS Energy Lett.* **2018**, *3*, 1279.
[47] W. Shockley, W. T. Read, *Phys. Rev.* **1952**, *87*, 835.
[48] R. N. Hall, In *Physical Review*, AMERICAN PHYSICAL SOC ONE PHYSICS ELLIPSE, COLLEGE PK, MD 20740-3844 USA, **1951**, pp. 228–228.
[49] I. Levine, S. Gupta, T. M. Brenner, D. Azulay, O. Millo, G. Hodes, D. Cahen, I. Balberg, *J. Phys. Chem. Lett.* **2016**, *7*, 5219.
[50] C. Eames, J. M. Frost, P. R. F. Barnes, B. C. O'Regan, A. Walsh, M. S. Islam, *Nat Commun* **2015**, *6*, 7497.
[51] E. M. Hutter, G. E. Eperon, S. D. Stranks, T. J. Savenije, *J. Phys. Chem. Lett.* **2015**, *6*, 3082.
[52] T. J. Savenije, D. Guo, V. M. Caselli, E. M. Hutter, *Adv. Energy Mater.* **2020**, *10*, 1903788.
[53] Q. Wang, Y. Shao, H. Xie, L. Lyu, X. Liu, Y. Gao, J. Huang, *Appl. Phys. Lett.* **2014**, *105*, 163508.
[54] Q. He, G. Chen, Y. Wang, X. Liu, D. Xu, X. Xu, Y. Liu, J. Bao, X. Wang, *Small* **2021**, *17*, 2101403.